ELSEVIER

Journal of Fluids and Structures 24 (2008) 1313–1325

JOURNAL OF FLUIDS AND STRUCTURES

www.elsevier.com/locate/jfs

Coherent and turbulent process analysis in the flow past a circular cylinder at high Reynolds number

R. Perrin[a,*], M. Braza[b,*], E. Cid[b], S. Cazin[b], P. Chassaing[b], C. Mockett[c], T. Reimann[c], F. Thiele[c]

[a]*Laboratoire d'Etudes Aérodynamiques (LEA), Université de Poitiers, ENSMA, CNRS SP2MI, téléport 2, Bd Marie et Pierre Curie, BP 30179, 86962 Futuroscope Chasseneuil Cedex, France*

[b]*Institut de Mécanique des Fluides de Toulouse, Unité Mixte C.N.R.S.-I.N.P.T. 5502, Av. du Prof. Camille Soula, 31400 Toulouse, France*

[c]*Institut für Strömungsmechanik un Technische Akustik, TU-Berlin, Müller Breslau Str. 8, 10623 Berlin, Germany*

Received 31 March 2008; accepted 18 August 2008

Abstract

This article presents an experimental study of the turbulent flow past a circular cylinder at high Reynolds number by means of advanced optical measurements techniques. Following previous studies using standard PIV and stereoscopic PIV (3C PIV), TRPIV and 3C-TRPIV have been employed in low subsonic wind tunnel environment. The database consisting of statistical and time-dependent fields aims at providing a physical analysis of the coherent and turbulent part, as well as a proper basis for validation and improvement of recent turbulence modelling approaches for strongly detached flow at high Reynolds number. As the nonlinear interaction between the coherent and turbulent dynamics have to be taken into account in a model, particular attention is paid to a decomposition of the flow into a coherent and a turbulent part, and to the analysis of their dynamics. This is achieved both using phase averaging and Proper Orthogonal Decomposition. For phase averaging, the two first POD coefficients are used for the evaluation of the vortex shedding phase angle. Furthermore, selected results of a Detached Eddy Simulation which had been validated by means of the experiment, are also presented to contribute to the physical analysis. The present study's experimental data resolved in space and time allow the confirmation of the conditional averaging for the turbulent stresses evaluation, by alleviating their overestimation due to phase jitter that occurs between the trigger signal and the velocity, when the phase angle is determined from a wall pressure signal. A more accurate physical analysis of the flow is achieved, particularly regarding the occurrence of irregular vortex shedding.

1. Introduction

The physical analysis of high Reynolds turbulent flows around bluff bodies has been the object of a great deal of experimental work since the 1950s. Modern optical measuring techniques developed in the last decade provide a new insight in the flow physics concerning the separation and vortex shedding, by giving access to velocity fields in a way similar to the numerical simulation. Furthermore, the accurate prediction of unsteady turbulent flows past bluff bodies

*Corresponding authors.
E-mail addresses: rodolphe.perrin@lea.univ-poitiers.fr (R. Perrin), braza@imft.fr (M. Braza).

0889-9746/$ - see front matter © 2008 Elsevier Ltd. All rights reserved.
doi:10.1016/j.jfluidstructs.2008.08.005

at high Reynolds number remains a very challenging task, given the inability of the Large Eddy Simulation (LES) to properly resolve the near wall region, that limits this approach to low Reynolds numbers. The statistical turbulence modelling approaches (URANS—Unsteady Reynolds Averaged Navier–Stokes) offer robustness and need reasonable grid sizes but they are often quite dissipative and damp the global instability and the coherent structures governing the flows around bluff bodies. Therefore, there is a need for development of advanced statistical approaches, able to capture the flow physics in the near region, to be used as 'stand alone' improved URANS, or in the context of hybrid URANS-LES, as for example in the Detached Eddy Simulation (DES). The present study is a continuation of previous studies of ours that used low data rate PIV, to analyse the coherent and turbulent processes in the detached flow past a circular cylinder at high Reynolds number. The circular cylinder configuration was chosen because of the strong separation and development of coherent structures, as well as the quasi-antisymmetric character of the global instability and of the alternating vortices, which allows well adapted processing and a better visualisation of the flow.

With the aim of allowing direct comparison possible with simulations, and therefore turbulence modelling validation, the cylinder was placed in a confined environment (a square channel) with a high blockage coefficient and a low aspect ratio, to enable CFD studies to use exactly the same flow domain as in the experiment by means of a reasonable grid size and to avoid, therefore, 'infinite' spanwise lengths. For this reason, this flow configuration has been used in the DESIDER European research program (Detached Eddy Simulation for industrial aerodynamics).

The challenging aspects of the present flow consist of strong separation and of the development of coherent structures interacting non-linearly with the turbulent motion. This dual physical nature, organised and turbulent, has to be analysed in detail to better understand the related physics, and therefore to take them into account in the modelling approach. This physical investigation is the main objective of the present paper.

In previous studies, the experiments were conducted using pressure measurements, PIV, stereoscopic PIV and Time Resolved PIV, carried out near the separation and in the very near wake of the cylinder (Perrin et al., 2006). The main limitation concerning the TRPIV measurements was the size of the domain which was smaller than that of the low data rate acquisitions, due to the low energy of the laser used. Particular attention was paid to the decomposition of the flow into a coherent part and a turbulent part. To this purpose, phase averaging, using pressure on the cylinder as a reference signal, and POD were first applied and compared. Both decompositions were analysed with the help of TRPIV measurements in a small domain. This was achieved by estimating the contributions of coherent and turbulent fluctuations to the Reynolds stress tensor. These contributions were evaluated first by simply interpolating and integrating the continuous part of the velocity spectra. They were compared with the respective contributions evaluated from the phase averaging decomposition [triple decomposition Reynolds and Hussain (1972)] and from the POD by considering different number of modes. It has been found, in agreement with other studies [e.g. Cantwell and Coles (1983)], that phase averaging with pressure leads to an overestimation of the turbulent motion and a smoothing of the von Kármán vortices, resulting from phase jitter that occurs randomly, between the pressure and the velocity signal in the wake. On the other hand, POD was found useful in analysing the different parts of the flow, but the main difficulty lies in the choice of the modes to reconstruct the coherent motion. It is noticeable that the measurement domain of TRPIV was too small to allow a relevant POD, and therefore, POD could only be performed on the low data rate acquisitions. An enhancement of the phase averaging was then achieved, using a definition of the phase angle based on the first two POD coefficients, and thereby alleviating the phase lags effects as the phase is determined directly from the velocity fields to be averaged. This phase averaging was obtained from low data rate PIV.

In this paper, complementary time resolved data sets are analysed. The main part of the analysis is based on Time Resolved PIV measurements, which have been carried out in a domain of similar size to that of the low data rate PIV, using a cylinder of smaller physical size and a laser delivering more energy. Also, a transverse plane is measured by 3C-TRPIV, to illustrate the 3-D flow structure. Moreover, a DES performed on a domain that corresponds precisely to the experiment, and which have been found to be in good agreement with the measurements (Perrin et al., 2007c), is also used as a complement for the analysis.

Section 2 briefly presents the configuration of the flow and the new measurements carried out, together with comparisons with previous measurements. In Section 3, the instantaneous motion is analysed. Section 4 is devoted to the analysis of the POD performed on the new data set. Finally, an analysis of coherent and incoherent quantities is conducted in Sections 5 and 6.

2. Configuration and experimental set-up

The experiments have been conducted in the IMFT's wind tunnels S1 and S4. As mentioned in the previous section, a high blockage coefficient and a low aspect ratio were employed to allow comparisons with simulations carried out on a domain corresponding precisely to the experimental geometry without the use of infinite boundary conditions.

Concerning the previous measurements in S1, the cylinder had a diameter of 14 cm and was placed in a square channel of cross-section 67×67 cm, leading to a blockage coefficient of $D/H = 0.21$ and an aspect ratio of $L/D = 4.8$. The inlet velocity was $U_0 = 15\,\mathrm{m\,s^{-1}}$ and the Reynolds number was 140 000. Due to the low energy of the laser used, and to the access of the wind tunnel, the previous TRPIV measurements were limited to a small domain. To carry out TRPIV on a larger domain in the wake, the new measurements have been done in the wind tunnel S4 of IMFT, having a cross-section of 61×71 cm. To keep the same blockage coefficient as in the previous measurements, the diameter of the cylinder was chosen 12.5 cm, which results in a blockage coefficient of 0.21 and an aspect ratio of 5.7. The Reynolds number was kept to 140 000, using an inlet velocity $U_0 = 16.8\,\mathrm{m\,s^{-1}}$. Although the aspect ratio is different from the previous one and therefore the flow was not expected to be rigorously the same, it has been seen that a good agreement with the old measurements is achieved for the mean flow and the velocity spectra.

A detailed description of the former measurements by low data rate PIV can be found in Perrin et al. (2007b), as well as the procedure used for the reconstruction of the three components in stereoscopic measurements. The new TRPIV measurements have been done using a laser Darwin 2×20 mJ from Excel Technology, a camera CMOS APX (PHOTRON) with a resolution of 1024×1024 pixels, and DEHS as seeding particles (typical size 1 μm). The system allowed acquisition of image pairs at a rate of 1 kHz. The image pairs were analysed using an in-house code 'PIVIS' developed by the 'Services Signaux Images' of IMFT, which uses an algorithm based on a 2-D FFT cross correlation function implemented in an iterative scheme with a sub-pixel image deformation (Lecordier and Trinite, 2003). The flow was analysed by cross-correlating 50% overlapping windows of 32×32 pixels, yielding fields of 61×57 vectors with a spatial resolution of 3 mm ($0.0238D$). Approximately 2% of the calculated vectors were detected as outliers using a sort based on the norm, the signal-to-noise ratio, and a median test filter, and these vectors were replaced using a second order least square interpolation scheme. Six temporal series of 3072 images pairs have been acquired and analysed, each series containing approximately 85 vortex shedding periods. The 3C-TRPIV presented in the following section has been performed using a Pegasus laser from New-Wave which delivers $2 * 10$ mJ at 1 kHz and two cameras CMOS RS3000 (Photon) with a resolution of $1024 * 1024$ pixels used in the Scheimpflug angular configuration.

Comparisons between these new TRPIV measurements and the former measurements have been made in Perrin et al. (2007a), given the small differences in the experimental set-up. Although not shown here, the recirculation length is found to be 1.25 and agrees well with the value of 1.28 found with low data rate PIV. Comparison of velocity spectra at the same points issued from the new TRPIV measurements and TRPIV performed in the S1 wind tunnel have also shown good agreement. Therefore, the influence of the aspect ratio slightly modified compared with the previous studies is found to not have an important effect in the middle span plane.

The numerical results presented in the paper have been achieved by a DES Simulation, performed on a domain that corresponds precisely to the experimental geometry. This simulation had been previously validated comparing with the experiment, using time averaging, phase averaging (with pressure trigger signal) and POD, in Perrin et al. (2007c), and was presented in detail in a companion paper (Mockett et al., 2007). Therefore, the numerical detail are not presented here. The analysed data set consists of 14 000 instantaneous snapshots, corresponding to approximately 90 vortex shedding periods, the dimensionless time step being $\Delta t^* = \Delta t U_0/D = 0.0321$.

3. Instantaneous motion

Fig. 1 shows a sequence of instantaneous superimposed vorticity and velocity, corresponding approximately to half a period (one picture in every three is represented as well as one velocity vector in every two). The vortex shedding is clearly shown, together with smaller vortices in the separated shear layer which are wrapped around the Kármán vortices. This behaviour is in good agreement with the measurements of Leder and Brede (2004) at a lower Reynolds number, although the flow is more irregular, as could be expected at this high Reynolds number. The same temporal behaviour is found in the DES simulation (e.g. Fig. 10).

A 3-D representation of the motion is provided in Fig. 2, where instantaneous fields from Stereoscopic Time Resolved PIV and by the DES are shown. It is clearly seen that the main structures of the flow are the von Kármán vortices, the Kelvin Helmoltz vortices and longitudinal vortices connecting the von Kármán ones. These counter-rotating longitudinal vortices are issued from a secondary instability, as demonstrated in a number of studies, especially using DNS [e.g. Braza et al. (2001)], and have been studied experimentally at lower Reynolds numbers [e.g. Lin et al. (1995)]. For the stereoscopic TRPIV, the instantaneous fields on the (x, z) plane have been phased with the phase averaged motion on the (x, y) plane, allowing the tracking of the longitudinal vortices with respect to the von Kármán ones. In the following, the paper is more particularly devoted to the analysis of the von Kármán and chaotic motions in the (x, y) plane.

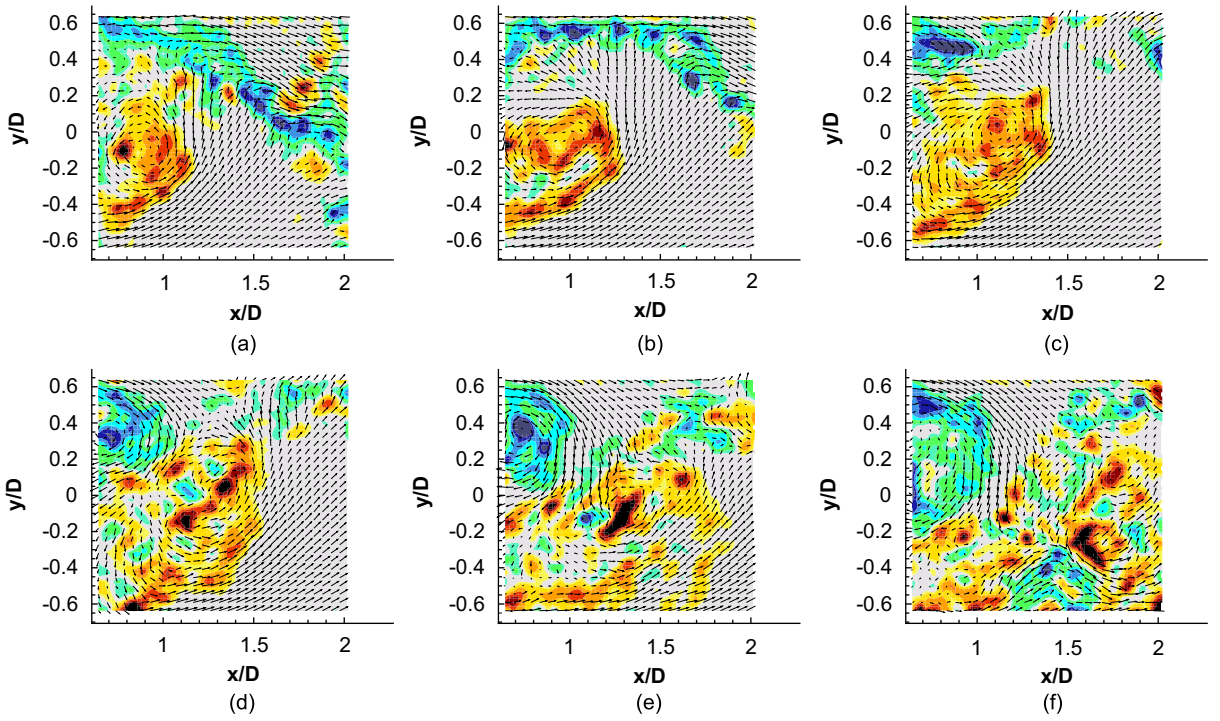

Fig. 1. Sequence of instantaneous fields (TRPIV). (a) $t = 9.1392$; (b) $t = 9.5424$; (c) $t = 9.9456$; (d) $t = 10.3488$; (e) $t = 10.752$; (f) $t = 11.1552$.

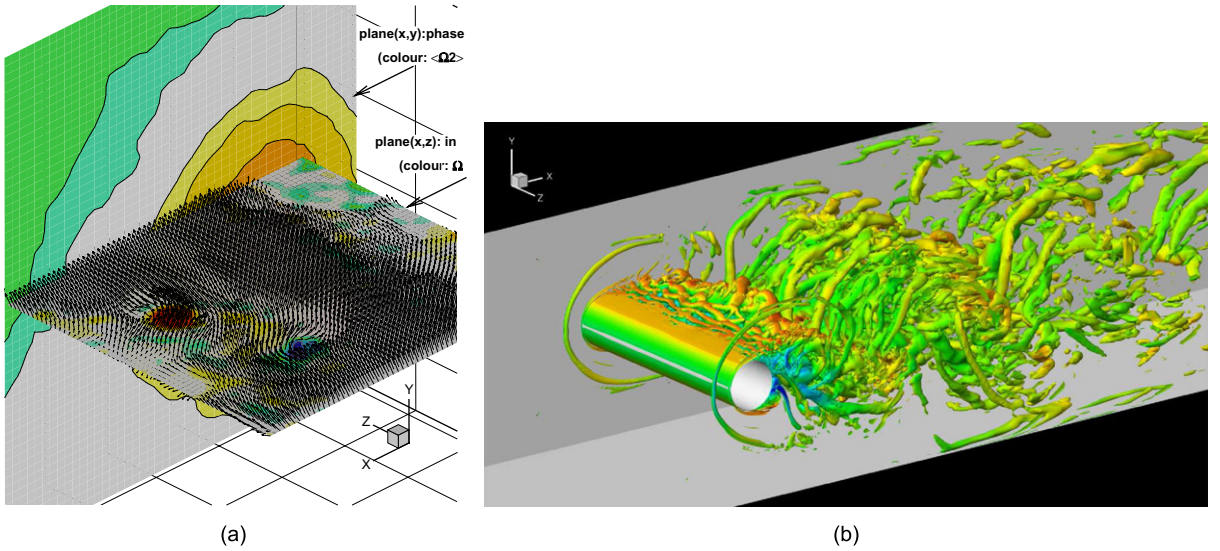

Fig. 2. Three dimensionality of the flow. (a) Stereoscopic time resolved measurements in (x, z) plane; (b) 3-D instantaneous fields issued from the DES.

The time signals of velocity in the near wake and of the wall pressure on the cylinder issued from the experiments and the simulation are shown in Fig. 3. Even if care must be taken when comparing directly these signals (the TRPIV signal results from the spatial and temporal filtering effects of the PIV, while the DES signal is a solution from modelled equations), they both present a number of similar features. Both signals classically exhibit a strong quasiperiodic component corresponding to vortex shedding, and a random component which is attributed to the turbulent motion. It

also appears that some irregularities are present at certain instants (Fig. 3 at $t^* \simeq 350$ and $t^* \simeq 400$ for the DES and $t^* \simeq 240$ for the experiment). During this phenomenon, which does not appear with a particular frequency, the quasiperiodic component seems to vanish. The impact of these irregularities on the vortex shedding will be analysed in more details in the following sections.

The velocity spectra issued from TRPIV, are shown in Fig. 4 for different locations. They classically exhibit a fundamental frequency peak and harmonics linked with the vortex shedding, as well as a continuous part corresponding to the turbulent motion. The sampling rate does not enable capturing distinct frequency peaks of smaller classes of coherent structures appearing in the near-wake. As expected, due to the absolute character of the von Kármán instability, the peak corresponding to the vortex shedding is found at the same dimensionless frequency at every point

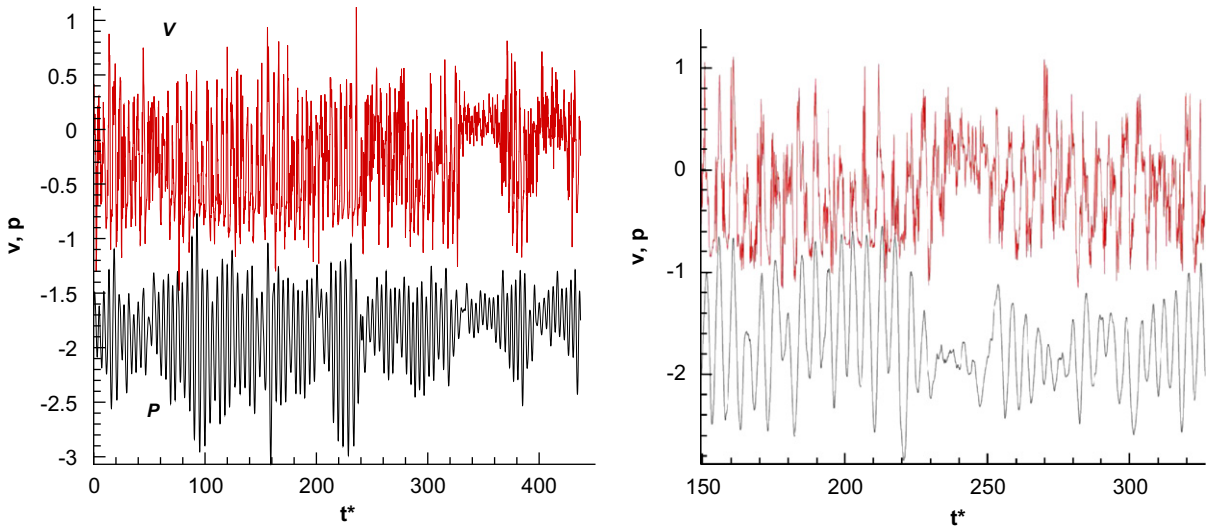

Fig. 3. Time signal of V velocity at $x/D = 1$, $y/D = 0.5$ and of the pressure signal at $\theta = 70^\circ$ from the simulation (left) and the experiment (right).

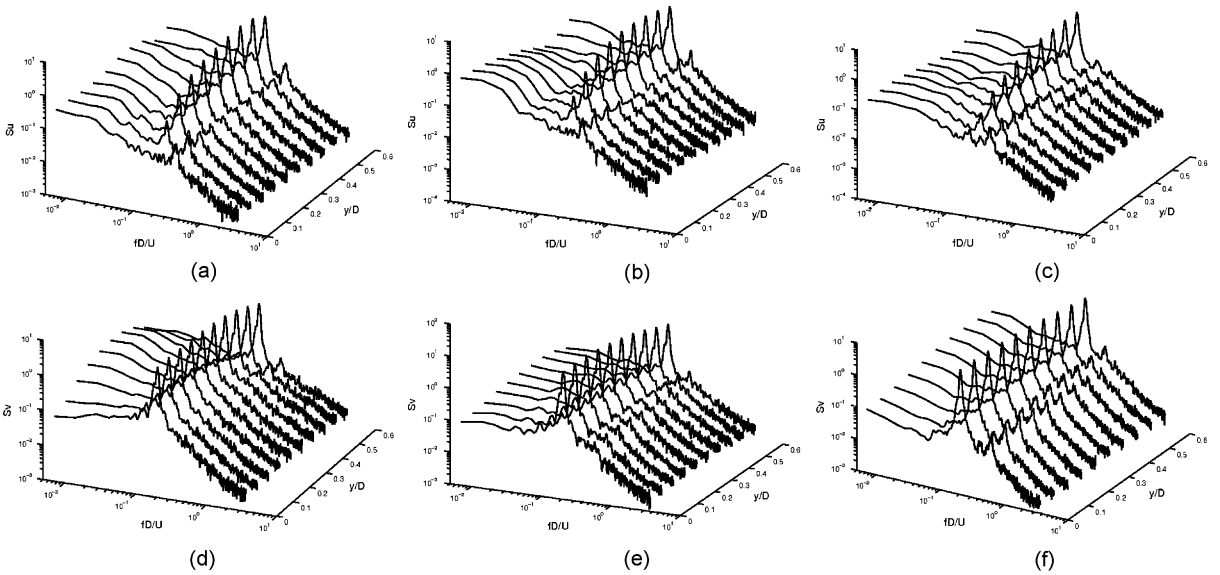

Fig. 4. Velocity spectra in the near wake (TRPIV). (a) U at $x/D = 0.5$; (b) U at $x/D = 1.3$; (c) U at $x/D = 2$; (d) V at $x/D = 0.5$; (e) V at $x/D = 1.3$; (f) V at $x/D = 2$.

(Strouhal number St = 0.21). On the rear axis, the first harmonic is predominant in the u spectrum due to the symmetry of the flow. It is also seen that the level of the second harmonic increases as x/D increases, especially for v component.

4. Proper Orthogonal Decomposition

The Proper Orthogonal Decomposition (Berkooz et al., 1993) has been applied on the TRPIV results and on the DES results. A complete description of POD can be found in Berkooz et al. (1993). In this study, POD is applied to the fluctuating motion and the following notations are adopted

$$\vec{u}(\vec{x},t) = \sum_n a_n(t)\vec{\Phi}_n(\vec{x}),$$

where $\vec{\Phi}_n(\vec{x})$ are the POD modes and $a_n(t)$ their associated coefficients. The access to spatio-temporal data allows the analysis of the temporal evolution of the coefficients associated with each POD modes. Furthermore, as the simulation gives access to the velocity in the whole domain, it is possible to study the influence of the domain on which is performed POD.

Fig. 5 shows the cumulative sum (percentage) of energy of the POD modes, as well as the shape of the first three modes, obtained from the TRPIV measurements. In agreement with other wake studies at lower Reynolds number (Noack et al., 2003; Deane et al., 1991 and others), the two first modes can be associated with the von Kármán vortices. Their topology is found to be very similar to that found at low Re. The higher-order modes however are more difficult to analyse. While, at low Reynolds number, the modes can be grouped by pairs and are related to the harmonics of the Strouhal frequency, it appears that higher-order modes, in our case, present different topologies to that observed at low Re and cannot be directly related to the harmonics of the Strouhal frequency.

To analyse these modes, time traces and spectra of the coefficients associated with each modes have been plotted. Fig. 6(b), (c) shows the spectra of the coefficients a_1 to a_{10}. As expected, the spectra of the first two coefficients are mainly dominated by a peak at the Strouhal frequency. The time traces of these two coefficients present a quasi-sinusoidal behaviour, a_1 and a_2 being shifted by a phase angle $\pi/2$ (Fig. 6(a)). This quasi-sinusoidal evolution is however modulated both in frequency and amplitude and the spectral peak displays a width. The other coefficients show a more complex behaviour. Although not shown for all modes here, their time traces appear very chaotic and their spectra present a non negligible continuous part. Some coefficients present distinct peaks at frequencies multiple of the Strouhal number, but it is not possible to identify clearly pairs of modes associated with the harmonics. The fact that the distinct frequencies are not clearly isolated by one pair of modes is of course not surprising given the highly turbulent character of the flow, but this is also due to the domain size influence, as will be seen in the following paragraph.

Even if the higher-order modes are not clearly identifiable, the behaviour of the third mode can be analysed, especially with respect to the instants of irregularities identified in the previous section. The spectrum of a_3 indicates that this mode is mainly characterised by low frequencies. Furthermore, looking at its time trace, its amplitude seems to increase during the instants where the shedding is irregular (Fig. 6(a) at $t \simeq 190$). This increase of a_3 is also associated with a diminution of the amplitude of a_1 and a_2.

The DES results can also be used to study the influence of the domain on POD. To this aim, the numerical data have been stored on a plane at midspan position and POD have been performed on three domain of increasing size, the smallest corresponding to the PIV measurements domain. Fig. 7 shows the first POD modes obtained for each domain. It is first observed that the modes are very similar to those issued from TRPIV on the smallest domain, confirming the

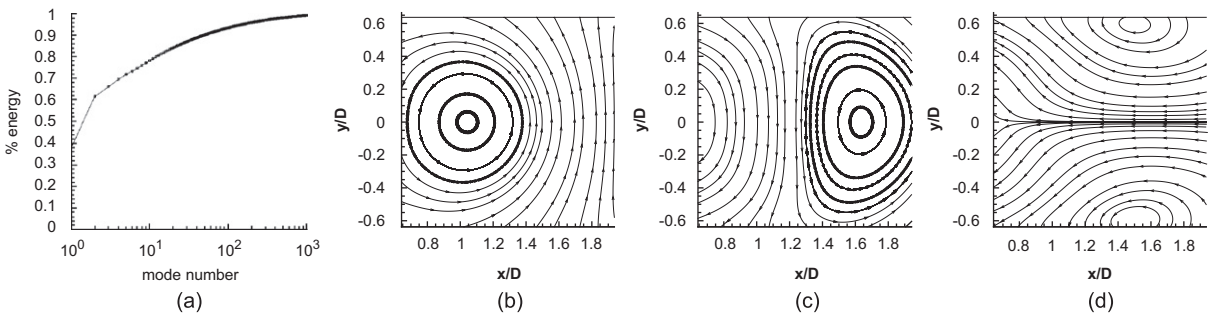

Fig. 5. POD modes (TRPIV). (a) Percent of energy of POD modes (b) Mode 1; (c) Mode 2; (d) Modes 3.

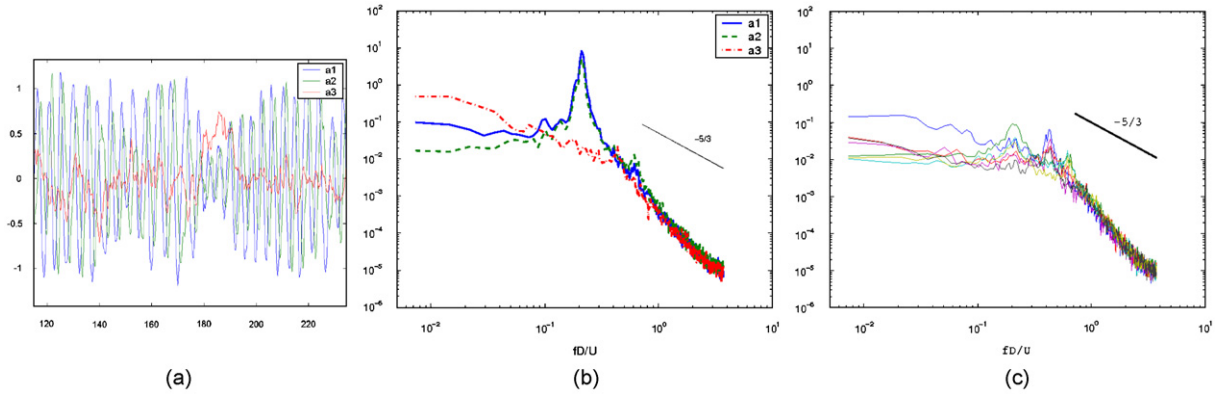

Fig. 6. Temporal behaviour of the POD coefficients (TRPIV). (a) POD coefficients a_1, a_2 and a_3; (b) spectra of a_1, a_2 and a_3; (c) spectra of a_4 to a_{10}.

good agreement of the simulation with the experiment. The most striking feature is that when the whole domain is considered, four modes appear related to the shedding, instead of the first two in case of the small and medium domain. It appears, therefore, that POD is strongly dependent on the domain size. This comparison suggests that the spectral content of each mode observed in the previous paragraph is highly dependent on the domain. The third mode on the small domain appears similar to mode 5 on the large domain and it is seen that significant values of this mode appear only in the near region.

5. Phase averaging

The quasiperiodic character of the vortex shedding leads to use phase averaging for the analysis of the coherent and random fluctuations. According to Reynolds and Hussain (1972), the triple decomposition is considered:

$$U_i = \overline{U_i} + \tilde{U}_i + u_i', \tag{1}$$

where $\overline{U_i}$ is the time-independent mean flow, $\tilde{U}_i$ is the quasiperiodic fluctuating component, u_i' is the random fluctuating component, and $\langle U_i \rangle = \overline{U_i} + \tilde{U}_i$ is the phase averaged velocity. Therefore, it is possible to evaluate the phase averaged turbulent stresses $\langle u_i' u_j' \rangle$ that appear in the equations for $\langle U_i \rangle$.

This meets the objective of providing a database useful for turbulence modelling, where the use of phase averaging is particularly attractive because it allows both the evaluation of the coherent motion, and of the turbulent stresses that appear in the phase averaged Navier–Stokes and have to be modelled. It is however noticeable, that the irregularities observed in Section 3 have a strong impact on the processing to be used. Phase averaging needs the assumption that the vortex shedding repeats itself from one cycle to another. Therefore, a distinction has to be made between the instants of regular shedding and the instants where the shedding become irregular. In this section, only the instants during which the shedding is regular enough to be phase averaged are considered.

Phase averaging needs a reference signal to determined the phase of the shedding at each instant. In Perrin et al. (2007b), this was done using the pressure signal on the cylinder at $\theta = 70^\circ$ as a trigger signal. In Perrin et al. (2006), it was shown that due to phase lags occurring at certain instants between the pressure signal and the velocity in the wake, a residual periodic component remained in the 'random fluctuation' part, the spectra of which exhibited a small peak in addition to the continuous part. As a result, the contribution of the coherent motion to the time-independent Reynolds stresses was underestimated and the contribution of the random motion was overestimated. To alleviate this problem, the phase angle was then defined using the coefficients associated with the two first POD modes, following BenChiekh et al. (2004) and van Oudheusden et al. (2005). It was shown that the vortices were less smeared by the averaging, and that the level of the contribution of the 'random motion' to the time-independent Reynolds stresses was diminished. The TRPIV data of this study, resolved in space and time, allow the study of the time evolution of the POD coefficients and thereby the phase angle defined in this way. Therefore, the efficiency of the corresponding phase-averaged decomposition is evaluated from a spectral point of view.

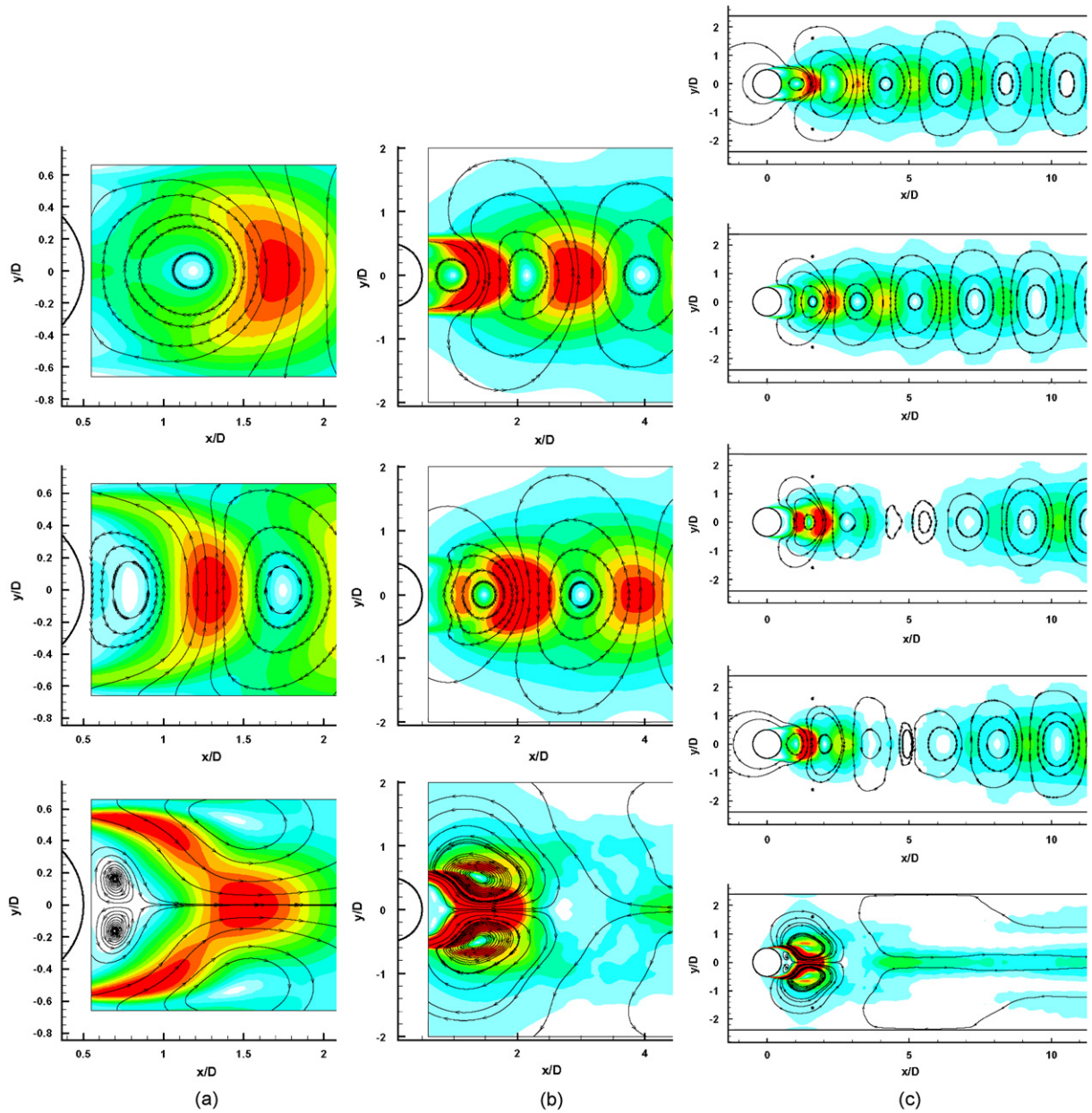

Fig. 7. Influence of the domain on POD (DES results). (a) PIV domain; (b) medium domain; (c) hole domain.

The temporal evolution of the first two coefficients, available from the present TRPIV measurements, and represented in Fig. 8(a), confirms the possibility of defining a phase angle representative of the vortex shedding using

$$\varphi_{\mathrm{POD}} = \arctan\left(\frac{\sqrt{2\lambda_2}\,a_1}{\sqrt{2\lambda_1}\,a_2}\right), \tag{2}$$

where λ_1 and λ_2 are the corresponding eigenvalues (it is recalled that $\overline{a_n^2} = \lambda_n$). The time evolution of this phase angle is also represented in this figure. As this phase angle is defined directly from the velocity to be averaged, the effects of the phase lags occurring between the reference signal and the velocity are expected to be alleviated.

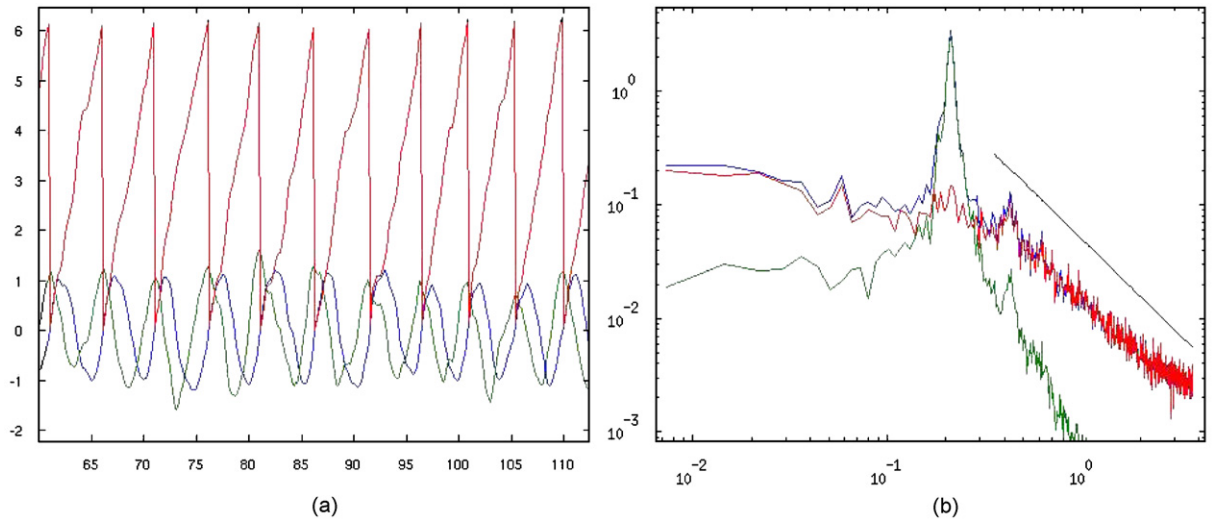

Fig. 8. Phase averaging (TRPIV). (a) Time evolution of coefficients a_1, a_2 and φ_{POD}; (b) spectrum of v (blue line), $\tilde{v}$ (green line) and v' (red line) at $x/D = 1.5$, $y/D = 0.5$.

For the phase averaging, the instants where the shedding is irregular, as discussed in the previous paragraph, have to be detected and removed from the averaging procedure. As a low amplitude of the first two POD coefficients is observed during these instants, this was achieved by applying a threshold to $\sqrt{a_1^2 + a_2^2}$. Approximately 20% of the signal was rejected.

The resulting phase averaged motion and fluctuation away from this phase average can be examined from a spectral point of view. Fig. 8(b) shows spectra of $\tilde{v}$ and v' at $x/D = 1.5$ and $y/D = 0.5$. A significant reduction of the residual peak in the v' spectrum is achieved using POD coefficients, confirming that the effects of phase jitter are alleviated.

A comment is necessary with respect to the domain on which is performed POD. It has been shown in Section 4 that the peak in the spectra is well represented by the two first POD modes when using a region extended up to approximately 5-D. Taking a larger region leads to obtain a higher number of modes linked with the von Kármán vortices, and it would be difficult to define a phase angle in this case. However, the definition of a phase angle when POD is performed in the near-wake still allows the phase averaging on all the domain. In this case, it is not expected that the phase jitter effects are alleviated in the far wake. Although not shown here, this procedure has been applied to the numerical data set and the results appear similar to those achieved for the experiment in the near-wake (i.e. a reduction of the overestimation of the turbulent stresses).

The experimental phase averaged fields are presented in Fig. 9. The phase averaged velocity, the $\langle \Omega_{21} \rangle$ component of the rotation rate tensor, the turbulent stresses issued from 2C-PIV and 3C-PIV, are shown, as well as the turbulent kinetic energy and the production term at phase angle $\varphi = 45°$. On each figure, the red line corresponds to the iso-contour 0.5 of the Q criterion, used to identify the vortices.

$\langle \Omega_{21} \rangle$ clearly exhibits the vortex shedding. The maximum value at the centre of the vortices is of order 3 at $x/D \simeq 1$ during their formation and decreases to 2 at $x/D \simeq 2$ at the beginning of their convection. $\langle u^2 \rangle$ and $\langle uv \rangle$ have their highest values in the shear regions near the separation. When the vortices are formed, the two lobes of high values of $\langle u^2 \rangle$ are transported towards the rear axis, and the centre of the vortices. At the beginning of the convection, the highest values of $\langle uv \rangle$ are located in the shear regions near the saddle points between the vortices, where the strain rate is important. Concerning the normal stresses in the near-wake, they all exhibit their highest values near the centres of the vortices when they start to be convected. High values of $\langle v^2 \rangle$ and $\langle w^2 \rangle$ are also present between the vortices, and can be supposed to be linked to the presence of longitudinal vortices connecting the primary one (cf. Fig. 2). Finally, regions of low turbulent stress values are identified in front of the vortices, corresponding to external fluid entering in the wake. It is also noticeable that a strong anisotropy is observed. The general topology of the stresses is found in good agreement with previous studies in wakes (Cantwell and Coles, 1983; Leder, 1991; Hussain and Hakayawa, 1987, among others). With the use of stereoscopic PIV, the turbulent kinetic energy k can be evaluated without assumption on $\langle w^2 \rangle$. Its topology is compared to the production term that appears in the k transport equation $P = -\langle u_i u_j \rangle (\partial \langle Ui \rangle / \partial x_j)$. It appears, in agreement with the aforementioned studies, that while the production is mainly located near the saddle

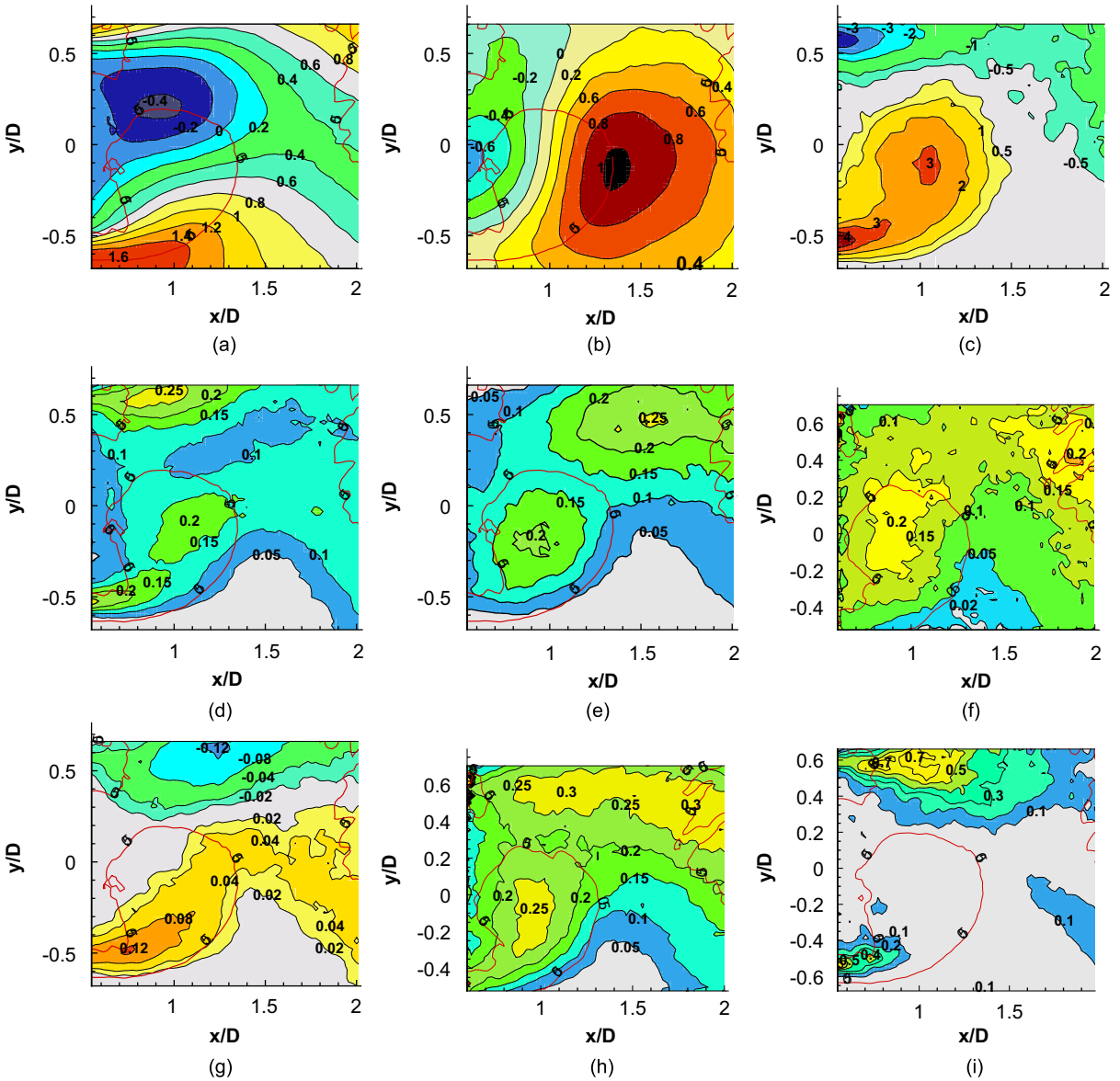

Fig. 9. Phase averaged quantities at $\varphi = 45°$. (a) $\langle U \rangle$; (b) $\langle V \rangle$; (c) $\langle \Omega_{21} \rangle$; (d) $\langle u^2 \rangle$; (e) $\langle v^2 \rangle$; (f) $\langle w^2 \rangle$; (g) $\langle uv \rangle$; (h) $\langle k \rangle$; (i) $\langle P \rangle$.

points in the shear regions, where the deformation rate and $\langle uv \rangle$ are important, the turbulent kinetic energy is mainly located near the centre of the vortices, suggesting a transport of the turbulent energy.

6. Analysis of the irregular shedding

It has been seen in Section 3 that at some instants, the periodic component, related to the vortex shedding, seems to vanish (Fig. 3). The vortex shedding is therefore affected and it is worth trying to analyse this phenomenon. As this phenomenon occurred both in the experiment and in the DES, we can look at the flow on a larger domain using the simulation. Fig. 10 (a) and (b) shows two instantaneous fields at times corresponding to (a) regular and (b) irregular shedding. It is observed that the von Kármán vortices are still present during the irregular instants but the formation of the vortices occurs farther downstream in the wake. The velocity signal at a position farther downstream still exhibits a periodic component. Although the fields are more "noisy" in the case of the experiment, a similar behaviour is observed on Fig. 10(c) and (d).

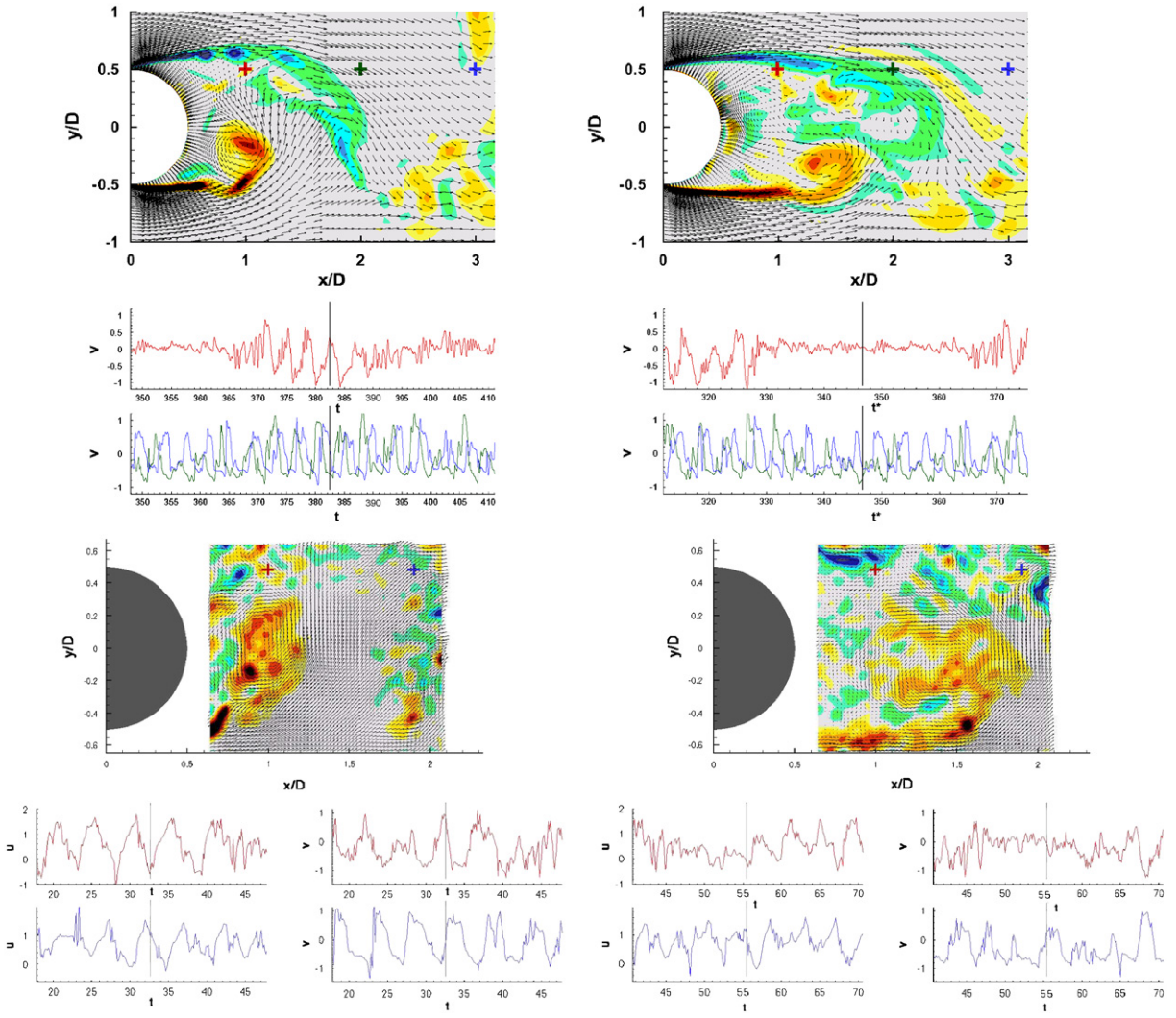

Fig. 10. Near wake behaviour at instants where the shedding is regular (left) and irregular (right). Top: DES, bottom: TRPIV.

The increase of the POD coefficient a_3 at these instants, observed in Section 4 can be related to this phenomenon. The topology of mode 3 (Fig. 5) presents similarities with the shift mode introduced by Noack et al. (2003) and Tadmor et al. (2007) for the flow past a cylinder at $Re = 100$. This mode is defined as the difference between the steady flow which presents a long recirculation region, and the mean flow which presents a short recirculation region. The extent of the region on which this mode is significant is smaller and more concentrated in the near-wake in our case. Mode 3 could act like the shift mode introduced in Tadmor et al. (2007) and could be associated with a slow variation of the wake structure, displaced in the longitudinal direction. Although further studies would be necessary to analyse the reasons of appearance of irregular vortex shedding 'spots', it seems that the intermittent increase of the formation region extent can be represented by the third mode evolution.

7. Conclusion and outlook

The near-wake of a circular cylinder at high Reynolds number has been experimentally studied using PIV, stereoscopic PIV and TRPIV, with the goal of providing a physical analysis of structural properties of turbulence affected by the coherent structure motion. Furthermore, the study provides a proper basis useful for validation and improvement of turbulence modelling for flows around bodies at high Reynolds number. While previous studies were

mainly based on low data rate PIV, this paper focuses on Time Resolved PIV measurements, which allow a spatio-temporal analysis of the flow. Specific results of a DES simulation in good agreement with the experiment were also used to complete the analysis. Concerning the decomposition of the flow into a coherent part and a turbulent one, the use of these data have confirmed the benefit of using POD coefficients to estimate phase averaged motion, because of the reduction of the jitter between the velocity to be averaged and the reference signal. This procedure allows the evaluation of the phase-averaged velocity component, as well as the phase averaged turbulent stresses, turbulent kinetic energy and production terms, appearing in the transport equations governing the phase averaged motion, used for efficient turbulence modelling in the present class of flows with a pronounced periodic character. Especially, TRPIV allowed a more complete description of the POD modes in this high Reynolds number range, by analysing the temporal evolution of their associated coefficients. Also, the occurrence of irregular vortex shedding has been identified and related with the intermittent extension of the vortex formation region farther downstream. This behaviour has been linked to the evolution of a low frequency POD mode.

Acknowledgements

The company "Excel Technology France" is gratefully acknowledged for loaning a Darwin PIV laser system. The authors also acknowledge the partial funding of the work presented here by the European Community during the DESider project in the 6th Framework Program, under Contract no. AST3-CT-2003-502842, and by the German Research Foundation (DFG) within the scope of the Collaborative Research Center SFB 557.

References

BenChiekh, M., Michard, M., Grosjean, N., Bera, J.C., 2004. Reconstruction temporelle d'un champ aéodynamique instationnaire à partir de mesures PIV non résolues dans le temps. In: 9^{e} Congrès Francophone de Vélocimétrie Laser.

Berkooz, G., Holmes, P., Lumley, J.L., 1993. The proper orthogonal decomposition in the analysis of turbulent flows. Annual Review of Fluid Mechanics. 25, 539–575.

Braza, M., Faghani, D., Persillon, H., 2001. Successive stages and the role of natural vortex dislocations in three-dimensional wake transition. Journal of Fluid Mechanics 439, 1–41.

Cantwell, B., Coles, D., 1983. An experimental study of entrainment and transport in the turbulent near wake of a circular cylinder. Journal of Fluid Mechanics 136, 321–374.

Deane, A.E., Kevrekidis, I.G., Karniadakis, G.E., Orzag, S.A., 1991. Low-dimensional models for complex geometry flows: Application to grooved channels and circular cylinders. Physics of Fluids A 3, 2337–2354.

Hussain, A.K.M.F., Hakayawa, M., 1987. Eduction of large-scale organized structures in a turbulent plane wake. Journal of Fluid Mechanics 180, 193–229.

Lecordier, B., Trinite, M., 2003. Advanced PIV algorithms with image distortion—Validation and comparison from synthetic images of turbulent flows. In: PIV03 Symposium, Busan, Korea.

Leder, A., 1991. Dynamics of fluid mixing in separated flows. Physics of Fluids A 3 (7), 1741–1748.

Leder, A., Brede, M., 2004. Comparisons between 3D-LDA measurements and TR-PIV data in the separated flow of a circular cylinder. In: 12th International Symposium on Applications of Laser Techniques to Fluid Mechanics. Lisbon, Portugal.

Lin, J.-C., Vorobieff, P., Rockwell, D., 1995. Three-dimensional patterns of streamwise vorticity in the turbulent near-wake of a cylinder. Journal of Fluids and Structures 9, 231–234.

Mockett, C., Perrin, R., Reimann, T., Braza, M., Thiele, F., 2007. Analysis of detached-eddy simulation for the flow around a circular cylinder with reference to PIV data. In: IUTAM Symposium on Unsteady Separated Flows and their Control, Corfu, Greece, 18–22 June.

Noack, B., Afanasiev, K., Morzynski, M., Tadmor, G., Thiele, F., 2003. A hierarchy of low-dimensional models for the transient and post-transient cylinder wake. Journal of Fluid Mechanics 497, 335–363.

Perrin, R., Braza, M., Cid, E., Cazin, S., Barthet, A., Sevrain, A., Mockett, C., Thiele, F., 2006. Phase averaged turbulence properties in the near wake of a circular cylinder at high Reynolds number using POD. In: 13th International Symposium on Applications of Laser Techniques to Fluid Mechanics. Lisbon, Portugal.

Perrin, R., Braza, M., Cid, E., Cazin, S., Chassaing, P., Mockett, C., Reimann, T., Thiele, F., 2007a. Coherent and turbulent process analysis in the flow past a circular cylinder at high reynolds number. In: IUTAM Symposium on Unsteady Separated Flows and their Control, Corfu, Greece, 18–22 June.

Perrin, R., Cid, E., Cazin, S., Sevrain, A., Braza, M., Moradei, F., Harran, G., 2007b. Phase averaged measurements of the turbulence properties in the near wake of a circular cylinder at high Reynolds number by 2C-PIV and 3-C PIV. Experiments in Fluids 42 (1), 93–109.

Perrin, R., Mockett, C., Braza, M., Cid, E., Cazin, S., Sevrain, A., Chassaing, P., Thiele, F., 2007c. Joint numerical and experimental investigation of the flow around a circular cylinder at high Reynolds number. Topics in Applied Physics, Particle Image Velocimetry, New Developments and Recent Applications 112, 223–244.

Reynolds, W.C., Hussain, A. K.M.F., 1972. The mechanics of an organized wave in turbulent shear flow. Part 3: Theoretical models and comparisons with experiments. Journal of Fluid Mechanics 54, 263–288.

Tadmor, G., Gonzales, J., Lehmann, O., Noack, B., 2007. Shift modes and transient dynamics in low order, design oriented galerkin models. In: 45th AIAA Fluids Conference and Exhibit, Reno, Nevada, USA, Paper 2007-0111.

van Oudheusden, B.W., Scarano, F., van Hinsberg, N.P., Watt, D.W., 2005. Phase-resolved characterization of vortex shedding in the near wake of a square-section cylinder at incidence. Experiments in Fluids 39, 86–98.